New modeling of the Vostok ice flow line and implication for the glaciological chronology of the Vostok ice core

New modeling of the Vostok ice flow line and implication for the glaciological chronology of the Vostok ice core

F. Parrenin,[1] F. Rémy,[1] C. Ritz,[2] M. J. Siegert,[3] and J. Jouzel[4]

Received 22 January 2004; revised 24 June 2004; accepted 22 July 2004; published 19 October 2004.

[1] We have used new spaceborne (elevation) and airborne (ice thickness) data to constrain a 2D1/2 model of snow accumulation and ice flow along the Ridge B-Vostok station ice flow line (East Antarctica). We show that new evaluations of the ice flow line geometry (from the surface elevation), ice thickness (from low-frequency radar data), and basal melting and sliding change significantly the chronology of the Vostok ice core. This new Vostok dating model reconciles orbital and glaciological timescales and is in good agreement with the Dome Fuji glaciological timescale. At the same time, the new model shows significantly older ages than the previous GT4 timescale for the last glacial part, being thus in better agreement with the GRIP and GISP2 chronologies. *INDEX TERMS:* 1827 Hydrology: Glaciology (1863); 3344 Meteorology and Atmospheric Dynamics: Paleoclimatology; 3260 Mathematical Geophysics: Inverse theory; 9310 Information Related to Geographic Region: Antarctica; *KEYWORDS:* glaciology, paleoclimatology, Antarctica, inverse theory

Citation: Parrenin, F., F. Rémy, C. Ritz, M. J. Siegert, and J. Jouzel (2004), New modeling of the Vostok ice flow line and implication for the glaciological chronology of the Vostok ice core, *J. Geophys. Res.*, *109*, D20102, doi:10.1029/2004JD004561.

1. Introduction

[2] Quaternary climate has been characterized by a succession of cold and warm periods with a periodicity of ~100,000 years, known as the glacial interglacial cycles [*Imbrie et al.*, 1992]. These cycles are largely documented by climatic records from deep sea sediments, continental sediments, pollens, loess, and deep polar ice cores. The records from deep ice cores are highly valuable, because there are long, continuous, and contain direct information on the past atmospheric composition, in particular concentration of greenhouse gases. The ice core that we investigate here, the Vostok ice core [*Petit et al.*, 1999], is the ice core that has been the most studied of all the available Antarctic ice cores. Even with the promising ice core drilled at Dome C [*EPICA Community Members*, 2004], the Vostok records will still be used, in particular to determine the limits of the interpretation of the Dome C data.

[3] Ice core dating is one of the principal challenges in the interpretation of ice core records. An accurate chronology is necessary to compare timing of variations of climatic proxies from an ice core with other paleoclimatic records or with insolation variations. Various methods can be used to date ice cores. They fall into four categories: (1) layers counting, (2) use of time markers and correlation with other dated time series, (3) comparison with insolation changes (i.e., orbital tuning), and (4) glaciological modeling. All these methods have advantages and drawbacks. Layer counting is not feasible when the annual layers thickness is too small to resolve visually. This unfortunately is the case in central Antarctica. At Vostok, the use of dated markers or time series is limited to the last tens thousands of years. Orbital tuning lies on the assumption that climate responds linearly to insolation variations, and has thus an uncertainty of about 6,000 years all along the records. Alternatively, glaciological modeling can be very powerful because it provides a chronology derived from physical equations which is consistent with some accumulation and thinning rates hypotheses, and which leads to realistic event durations. These models often contain poorly known parameters however, such as the glaciological conditions at the base of the ice sheet, or past accumulation rates. *Parrenin et al.* [2001] constrained the poorly-known parameters with independent chronological information, in the framework of an inverse method to establish the depth-age relationship of the Vostok ice core. Such work is a federative approach in the sense that it uses information coming from a variety of different methods (e.g., time markers, orbital tuning, and glaciological modeling). Even with relaxed modeling hypotheses, the federative chronology had some clear disagreements with other chronologies: (1) This chronology, when compared with the annually counted Greenlandic ice cores chronologies from GRIP and GISP2, was significantly younger by 4–6 kyr (thousand of years) for the last glacial period, 30–60 kyr ago. Because new records from speleothems, accurately dated by an U-Th method, roughly confirm these later chronologies [*Wang et al.*, 2001; *Genty et al.*, 2003], it is now clear that this discrepancy is due to a problem in the Vostok chronology. (2) There was a discrepancy of ~10 kyr

[1] Laboratoire d'Etudes en Geophysique et Océanographie Spatiales, Toulouse, France.
[2] Laboratoire de Glaciologie et Géophysique de l'Environnement, Saint Martin d'Hères, France.
[3] Bristol Glaciology Centre, School of Geophysical Sciences, Bristol, UK.
[4] Laboratoire des Sciences du Climat et de l'Environnement, Institut Pierre Simon Laplace, Gif-sur-Yvette, France.

0148-0227/04/2004JD004561

between orbitally tuned and glaciological chronologies between 250 and 300 kyr, forcing the restriction of the chronology to the last 220 kyr. (3) The duration of the last interglacial period (also known as stage 5.5 in marine records) was significantly longer with the glaciological chronology (16–17kyr) than with orbitally tuned chronologies (~12 kyr).

[4] The problem of modeling the ice flow into the Vostok ice core is more complicate than for other ice cores, because Vostok is not situated at a dome. The difference between the glaciological chronology and the other chronologies could thus be due to a poor representation of the ice flow line upstream of the ice core. In particular, the bedrock and surface topographic profiles between the Ridge B ice divide and Vostok were based on old map data from *Drewry* [1983a, 1983b]. New topographic data are now available for the surface from satellite [*Rémy et al.*, 1999], and for the bedrock from noninterpolated airborne radio echo sounding (RES) data [*Siegert and Kwok*, 2000]. In this article, we use these new data to improve the modeling of the Vostok ice flow line, and we study the consequences on the Vostok chronology.

2. Description of the Glaciological Dating Model Used

[5] To compute the age of the ice with respect to its depth, we need to estimate the rate of accumulation (A) and the thinning function (T), i.e., the ratio of the thickness of a layer to its initial thickness. The age of the ice at a given depth Z is then calculated through:

$$age(Z) = \int_0^z \frac{dy}{A(y)T(y)}. \tag{1}$$

The thinning function is evaluated through a flow model whereas the accumulation rate is computed by an accumulation model.

2.1. Flow Model

[6] Because the drilling site of the Vostok ice core is not located at an ice divide, a 1-D model is not sufficient to represent the true flow of the ice that makes up the Vostok core itself. However, a 3-D thermomechanical model, such as that designed to simulate the evolution of Antarctica [*Ritz et al.*, 2001], is both too heavy in computing time and does not have a sufficiently accurate resolution to date the Vostok ice core through an inverse method. Thus a simplified 2D1/2 model with imposed geometry is used to model the flow [*Ritz*, 1992]. This model is based on the order 0 of the shallow ice approximation [*Hutter*, 1983]. As a consequence, the direction of flow at any depth is supposed to follow the greatest surface slope direction. From the surface topography, it is thus possible to determine the positions of the ice flow lines (see section 3 for more details). These lines may not be parallel and we need to take into account their divergence (or convergence) in the mass balance equation.

[7] The mass balance equation is obtained by writing the balance of ice fluxes for an ice column whose sides are two adjacent ice flow lines. If the x direction is along the greatest slope, y direction is perpendicular, and if Y is the width between the two ice flow lines, we obtain:

$$\frac{\partial(\overline{U}_x H)}{\partial x} + \frac{H}{Y}\frac{\partial Y}{\partial x}\overline{U}_x = \dot{b} - \dot{f} - \frac{\partial H}{\partial t}, \tag{2}$$

where H is the ice sheet thickness, x the position along the ice flow line, $\overline{U}_x = \int_0^H u_x(z)dz$ is the horizontal velocity balance, $\dot{b}$ is accumulation rate at the top of the ice sheet, and $\dot{f}$ is the melting at the base of the ice sheet. We will note $Sh(x) = \frac{1}{Y}\frac{\partial Y}{\partial x}$, and thus $R_e = \frac{1}{Sh}$ is the curvature radius of isoaltitude lines, which can be easily obtained from the surface topography. Sh is positive for the divergence areas (for example at the domes), equal to zero when ice flow lines are parallel, and negative for the convergence areas (for example upstream of the outlet glaciers). We suppose in our model that the positions of the ice flow lines did not change during time: Sh is time-independent and equal to its actual value.

[8] The balance velocity $\overline{U}_x$ along the ice flow line can be calculated iteratively with equation (2), starting from the dome where it is equal to zero. To obtain the complete velocity field, the next step is the computation of the vertical velocity profile. By supposing that the temperature change linearly with depth, we can derive from the mechanical equations the following velocity profiles and thinning variations [*Ritz*, 1992]:

$$u_x(x,z) = \Psi(\zeta)\overline{U}_x \tag{3}$$

$$\begin{aligned} u_z(x,z) = {} & \left(\dot{b} - \frac{\partial H}{\partial t}\right)\left(1 - \int_0^\zeta \Psi(\zeta')d\zeta'\right) + \overline{U}_x\Psi(\zeta)\left(\zeta\frac{\partial H}{\partial x} - \frac{\partial E}{\partial x}\right) \\ & - \overline{U}_x H\left(\frac{\partial s}{\partial x}\int_0^\zeta \frac{\partial \Psi}{\partial s}(\zeta')d\zeta' + \frac{\partial m}{\partial x}\int_0^\zeta \frac{\partial \Psi}{\partial m}(\zeta')d\zeta'\right) \\ & + \dot{f}\int_0^\zeta \Psi(\zeta')d\zeta' - \frac{\partial B}{\partial t} \end{aligned} \tag{4}$$

$$\varepsilon_{zz} = -\overline{U}_x\frac{\partial \Psi}{\partial x} - \Psi\frac{\partial \overline{U}_x}{\partial x} - \overline{U}_x Sh(x)\Psi. \tag{5}$$

where $\zeta = \frac{Z}{H}$ is the relative depth, s (sliding) is the rate between the basal velocity and the mean velocity, m is a constant and Ψ is given by:

$$\Psi(\zeta) = s + (1-s)\frac{m+2}{m+1}\left(1 - \zeta^{m+1}\right). \tag{6}$$

Formulas for $\int_0^\zeta \Psi(\zeta')d\zeta'$, $\int_0^\zeta \frac{\partial\Psi}{\partial s}(\zeta')d\zeta'$, $\int_0^\zeta \frac{\partial\Psi}{\partial m}(\zeta')d\zeta'$ and $\frac{\partial\Psi}{\partial x}$ are given in Appendix A.

2.2. Accumulation Model

[9] Accumulation of snow principally results from precipitation of snow and from the redistribution of snow by wind at the surface [*Richardson et al.*, 1997]. Here we suppose that the rate of redistribution of snow by wind at a given position is constant through time, and that change in

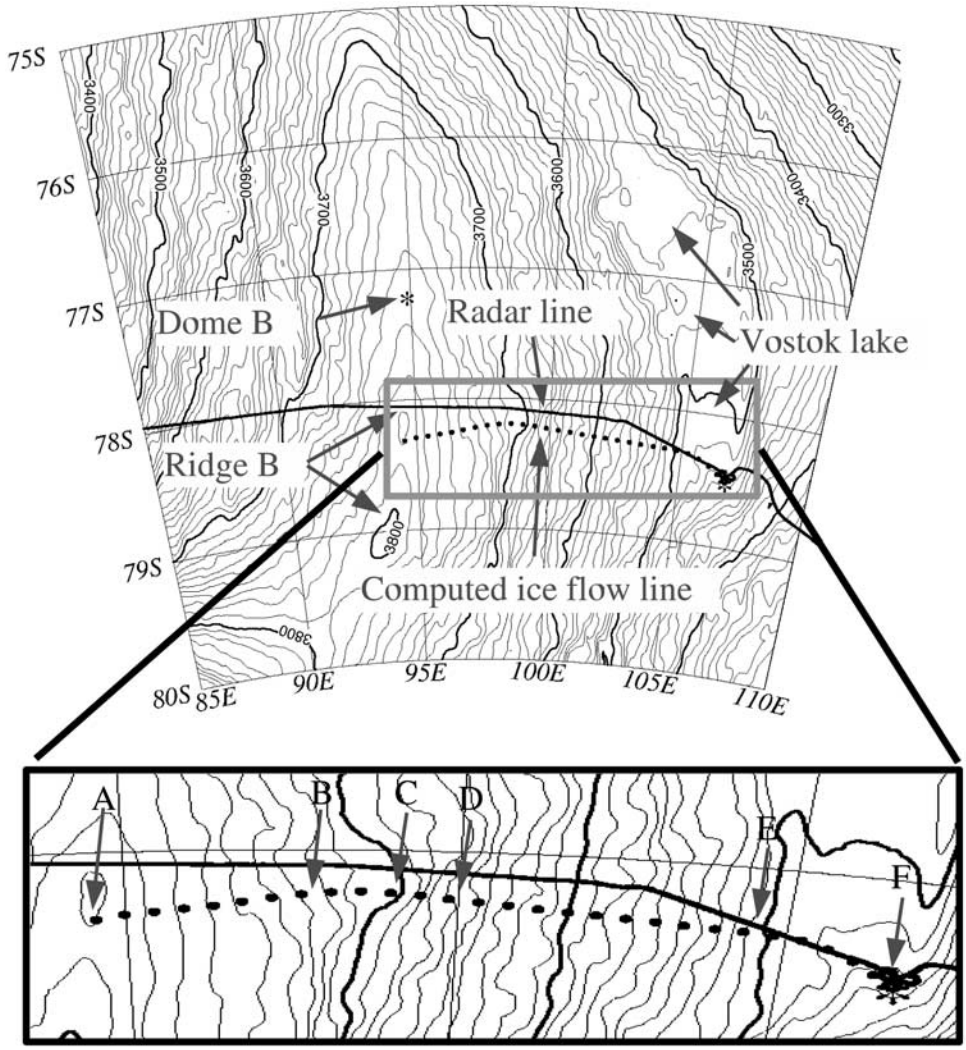

Figure 1. Position of the computed ice flow line (dotted line) compared with the position of the airborne radio echo sounding profile (plain line) from *Siegert and Kwok* [2000].

precipitation in central Antarctica are mainly governed by change in the mean temperature where precipitation forms, i.e., at the top of inversion layer (called the temperature of inversion). We can therefore show from a simple model of the air mass in the advective zone that variations of accumulation in central Antarctica can be deduced from the inversion temperature through [*Ritz*, 1992]:

$$A(x, T_I) = A^0(x)\frac{f(T_I)}{f(T_I^0)}\left(1 + \beta\left(T_I - T_I^0\right)\right), \tag{7}$$

where A is the accumulation rate, x is the position along the flow line, T_I is the inversion temperature, A^0 is the accumulation at a reference temperature T_I^0, β is a constant, f is a function given by:

$$f(T_I) = \frac{d}{dt}\left(\frac{P_S(T)}{T}\right)_{T=T_I} \tag{8}$$

where $P_S(T)$ is the saturation vapor pressure function of temperature. The constant β is for phenomena that are not linked to saturation vapor pressure, like changes in atmospheric wind intensity and changes in supersaturation (when the vapor pressure exceeds the saturation vapor pressure); here we suppose that it is constant in the Vostok area. $P_S(T)$ depends on temperature through an exponential relationship [*Ritz*, 1992]:

$$P_S(T) = A_S \cdot \exp\left(-\frac{B_S}{T}\right) \tag{9}$$

with P_S in Pa, T in K, A_S = 3.64149 · 1012 Pa, and B_S = 6148.3 K. (These values come from a best fit to the empirical curve of P_S over ice in the temperature range $-60°$ $-20°$C from Smithsonian tables). Past surface temperatures are estimated using the relationship between surface temperature (T_S) and isotopic composition (δD), and actual surface temperature (T_S^0) and isotopic composition (δD^0):

$$T_S = T_S^0 + \frac{\alpha}{6.04} \times \left(\delta D - \delta D^0\right) \tag{10}$$

The α parameter affects the amplitude of the change of temperature. A situation in which $\alpha = 1$ relates to the present day spatial relationship over Antarctica [*Lorius and Merlivat*, 1977]. Inversion temperature is then deduced from

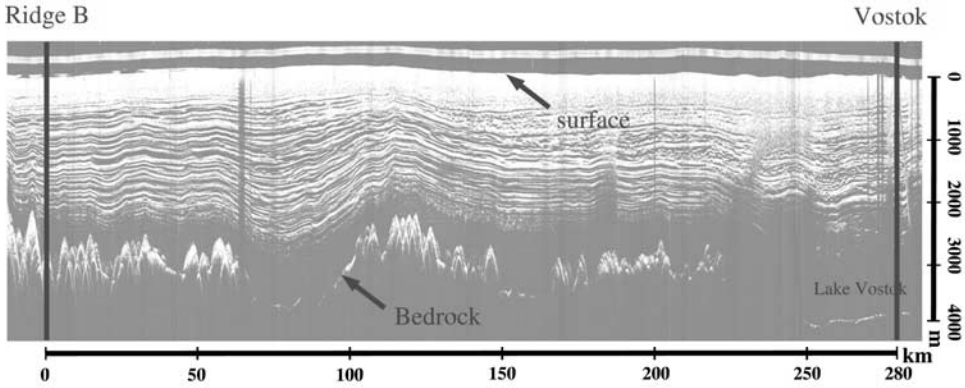

Figure 2. Radio echo sounding profile between Ridge B and the Vostok ice core site. After *Siegert and Kwok* [2000].

surface temperature through an empirical relationship [*Connolley*, 1996]:

$$T_I = 0.63 T_S + 88.9 \quad (T_I \text{ and } T_S \text{ in K}) \tag{11}$$

$A^0(x)$, α and β are free parameters of the accumulation model that will be reconstructed by the inverse method.

2.3. Firn Model

[10] The last step of the age model is the computation of gas bubbles age, which is different than the age of the surrounding ice because of firn porosity. The gas age/ice age difference is evaluated with a firn densification model [*Arnaud et al.*, 2000].

2.4. Numerical Aspect of the Dating Model

[11] Our model has a Lagrangian representation and runs backward in time. That is to say, we start from tracers placed regularly each meter in the Vostok deep drilling, and velocity equations give us iteratively the position of these tracers one time step before. Changes in thinning are integrated all along the ice trajectory until the tracer crosses the surface. This gives the spatial origin of the tracer, necessary to compute the accumulation.

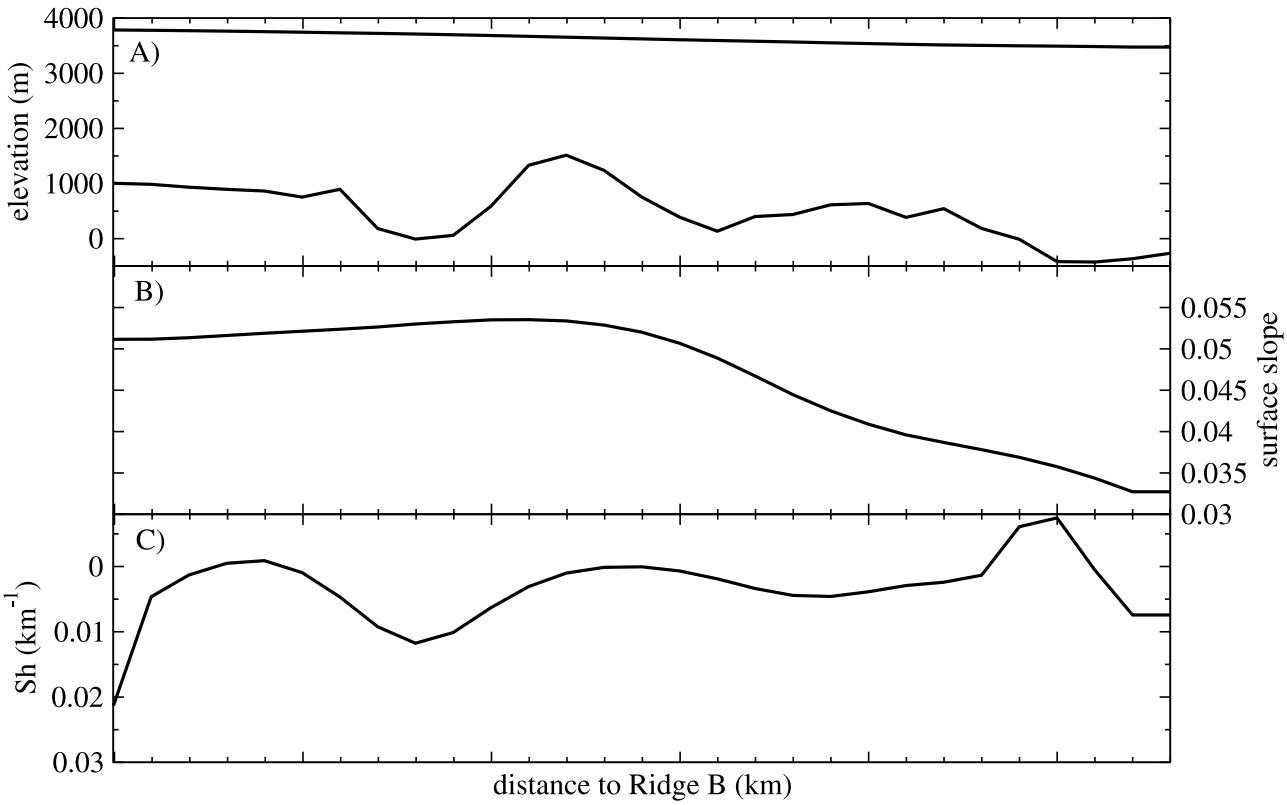

Figure 3. The Ridge B-Vostok ice flow line. (a) Bedrock and surface elevation. (b) Surface slope. (c) Sh parameter, measuring the divergence or convergence of ice flow.

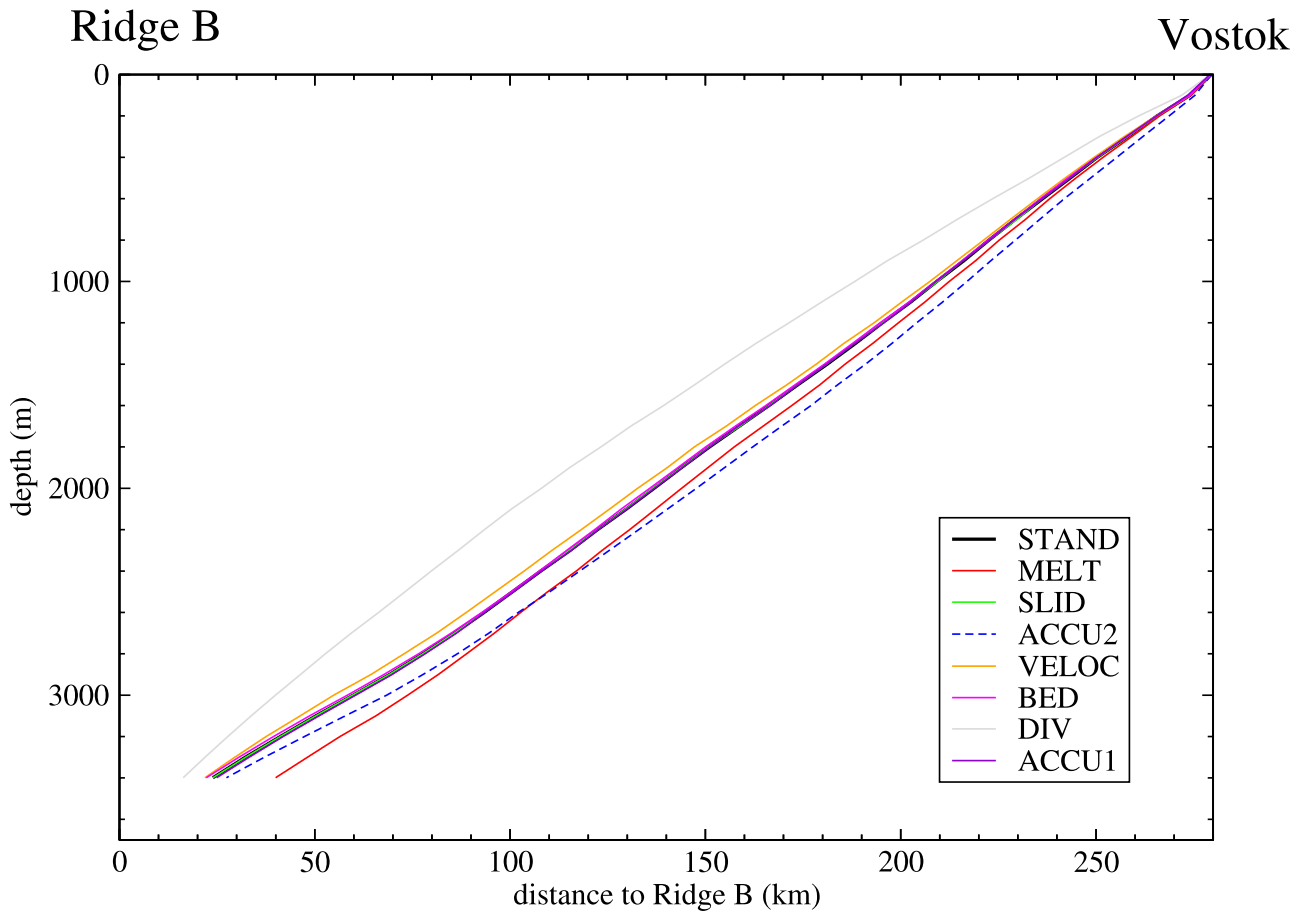

Figure 4. Origin of ice with respect to depth in the Vostok drilling in the different sensitivity experiments. Only divergence of ice flow, spatial accumulation variations, and melting rates have an important influence on ice origin.

[12] To compute ice velocity and thinning variations fields, we use an horizontal grid of 10 km and 41 vertical levels. Note that there is a circular problem in the model definition: the thinning model needs an accumulation history, which is based on a chronology for the Vostok drilling; the chronology itself depends on the thinning model. To circumvent this problem, we iterate several times on the thinning and accumulation models: starting from a preliminary timescale and preliminary accumulation rates, we compute ice particles trajectories, thinning factors and accumulation rates. These later allow us to compute a new chronology, and the new accumulation rates history is used as input for the subsequent iteration. We stop the process when the chronology converges, i.e., when adding a new iteration does not change significantly the chronology (4 iterations are generally sufficient).

3. Sensitivity Experiments

[13] To understand how the different model parameters influence the chronology of a deep ice core situated on an ice flow line, we performed several sensitivity experiments. Our primary reference experiment called STAND uses these parameters: (1) basal freezing above the Vostok subglacial lake (i.e., between E and F in Figure 1) of 1 mm/yr; basal melting equal to zero elsewhere; (2) basal sliding of 100% of total velocity above the Vostok lake; basal sliding equal to zero elsewhere; (3) present-day accumulation rates (A^0) equal to 3.1 cm of ice/yr in the first half of the ice flow line, and then linearly decreasing to 2.2 cm of ice/yr at the Vostok site; (4) m parameter from the velocity profile (see equation (4)) equal to 5 in the Ridge region (between 0 and 40 km far from Ridge B) and equal to 10 elsewhere; (5) horizontal bedrock profile from the radio echo sounding profile (Figure 2, see section 4); (6) divergence of ice flow based on the computation of adjacent ice flow lines from surface topography (Figure 3, see section 4). Several modeling experiments were then made in which we modified only one parameter: (1) MELT, basal melting upstream of Vostok lake was set to 1 mm/yr; (2) SLID, basal sliding upstream of Vostok lake was set to 20%; (3) ACCU1, present-day accumulation rate between Ridge B and Vostok (A^0) from STAND experiment was enhanced uniformly by a factor 1.5; (4) ACCU2, A^0 was set to 2.2 cm of ice/yr (i.e., the Vostok value) all along the flow line; (5) VELOC, the m parameter of the velocity profile was set to 5 all along the flow line; (6) BED, the bedrock elevation was supposed to be constant and equal to -265 m (i.e., the Vostok value) all along the flow line; (7) DIV, the divergence of ice flow was supposed to be null all along the flow line (i.e., parallel ice flow lines).

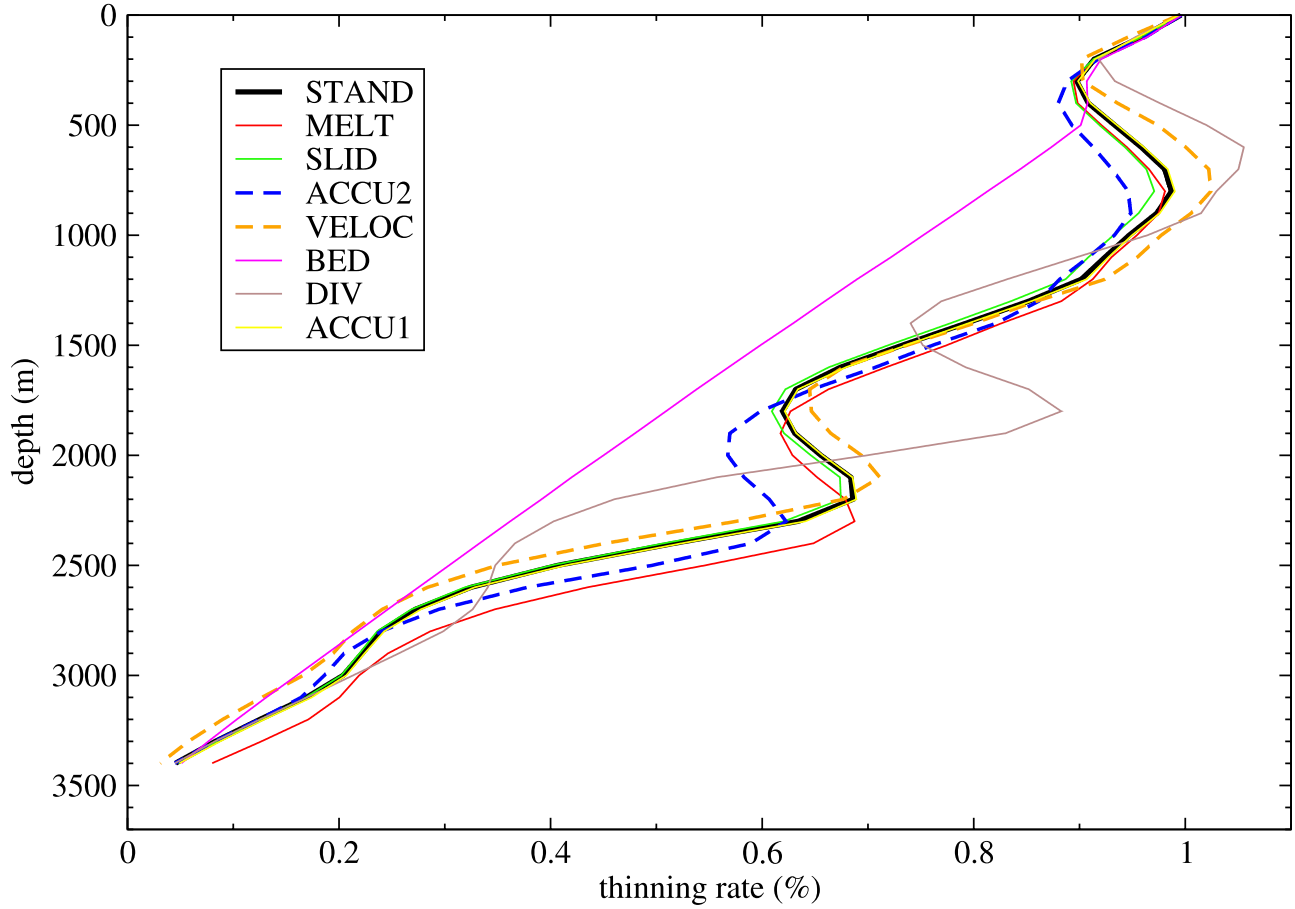

Figure 5. Thinning function versus depth for the Vostok deep drilling for the different sensitivity experiments. The clearest influence is horizontal bedrock profile which is directly imprinted on the vertical thinning profile. Melting rate, spatial accumulation variations, and divergence of ice flow have an influence on ice origin and thus on thinning profile if bedrock profile is not flat. Vertical velocity profile also has an important influence. Accumulation rates and sliding rates do not have an important influence.

In the following sections, we discuss the results of these various modeling experiments, and detail which processes influence the ice origin and the vertical thinning profile.

3.1. Ice Origin

[14] The ice origin with respect to depth for each experiment is shown in Figure 4. The first thing that we note is the quasi-linear feature of the ice origin versus depth. In a first approximation, the ice origin varies linearly between Vostok for the surface ice and Ridge B for the bottom ice. However, several parameters have a nonnegligible influence on ice origin. If we do not take into account divergence of ice flow (experiment DIV), ice originates significantly nearer to Ridge B than in the STAND experiment, the difference reaching ~30 km for 2000 m depth. Indeed, if we take into account the divergence of ice flow between Ridge B and Vostok, horizontal velocity is decreased and thus the proportion of vertical velocity is larger (and by consequence the slope of the ice particles trajectories is larger).

[15] The influence of accumulation rates is subtle, because an homogeneous enhancement of accumulation rate does not have an important influence (experiment ACCU1) but a change of the horizontal accumulation profile has a strong impact (experiment ACCU2). The ACCU2 experiment with a homogeneous accumulation rate upstream of Vostok leads to a maximum change in ice origin of ~10 km at 2000 m depth. The difference, however, is negligible for the surface and bottom parts.

[16] The MELT experiment, with a 1 mm/yr melting rate parameter upstream of the Vostok subglacial lake, leads to an ice which originates nearer to Vostok than in the STAND experiment, for ice at the same depth. Indeed, melting rate increases the vertical velocity and thus increases the slope of ice particles trajectories. We can note that the difference between STAND and MELT experiment roughly increases linearly with depth. The other parameters such as sliding, m from the vertical velocity profile, and horizontal bedrock profile have a negligible influence with respect to the three parameters discussed above.

3.2. Thinning Function

[17] The thinning function versus depth for each experiment is shown on Figure 5. The main feature of this profile is that it is strongly related to the bedrock profile upstream of Vostok: each mountain induces a perturbation in the vertical thinning profile. Indeed, when ice originates from a region where the ice thickness is small, the ice column has

Table 1. Age Control Points Used to Constrain the Vostok Timescale

	Depth, m	Age, years	Uncertainty, years
$^{10}Be/^{14}C$ age	178	7180	100
^{10}Be peak	601	41000	2000
Transition 6-5.5	1904	132400	6000
Transition 7.2-7.1	2516	200600	6000
Transition 8-7.5	2777	246000	6000
Transition 8.6-8.5	2945	293600	6000
Transition 10-9.3	3134	336200	6000
Transition 11.22-11.1	3218	373800	6000

globally expanded when it arrives at Vostok. Thus, in this case, the ice is less thinned by the time it arrives at the ice core site. Reciprocally, when the ice originates from a region with a large ice thickness, it has been more thinned. By consequence, if we do not take into account variations of bedrock elevation upstream of Vostok (experiment BED), vertical thinning function varies roughly linearly between 1 at surface and 0 at the base of the ice sheet.

[18] Of course, the *m* parameter of the vertical velocity profile has an influence on the thinning function (experiment VELOC), but with an opposite effect between the upper and the lower part of the ice core: a lower value for *m* leads to less thinning in the upper part and more thinning in the lower part.

[19] Basal conditions (melting and sliding, exp. MELT and SLID) have also an important influence on vertical velocity profile and thus on the thinning function. Spatial differences on basal conditions can thus lead to irregularities in the thinning function against depth.

[20] Some parameters have an indirect influence on the thinning function via the ice origin. Indeed, each parameter having an influence on ice origin influences also the vertical position of the bedrock and basal conditions fingerprints in the deep drilling. For example, the divergence of ice flow (*Sh*) has an negligible influence on the thinning function if bedrock elevation and basal conditions are homogeneous upstream of Vostok (experiment not shown here). However, if bedrock elevation or basal conditions are not homogeneous (as is the case upstream of Vostok), the divergence of ice flow has a strong influence on the thinning function. This is also true with the spatial distribution of accumulation rate. Melting and the *m* parameter have both a direct and an indirect influence on the thinning function.

[21] This sensitivity study shows clearly that a realistic parameterization of the glaciology is required in order to correctly evaluate the Vostok ice core chronology. It also reveals that the glaciological dating model for the Vostok

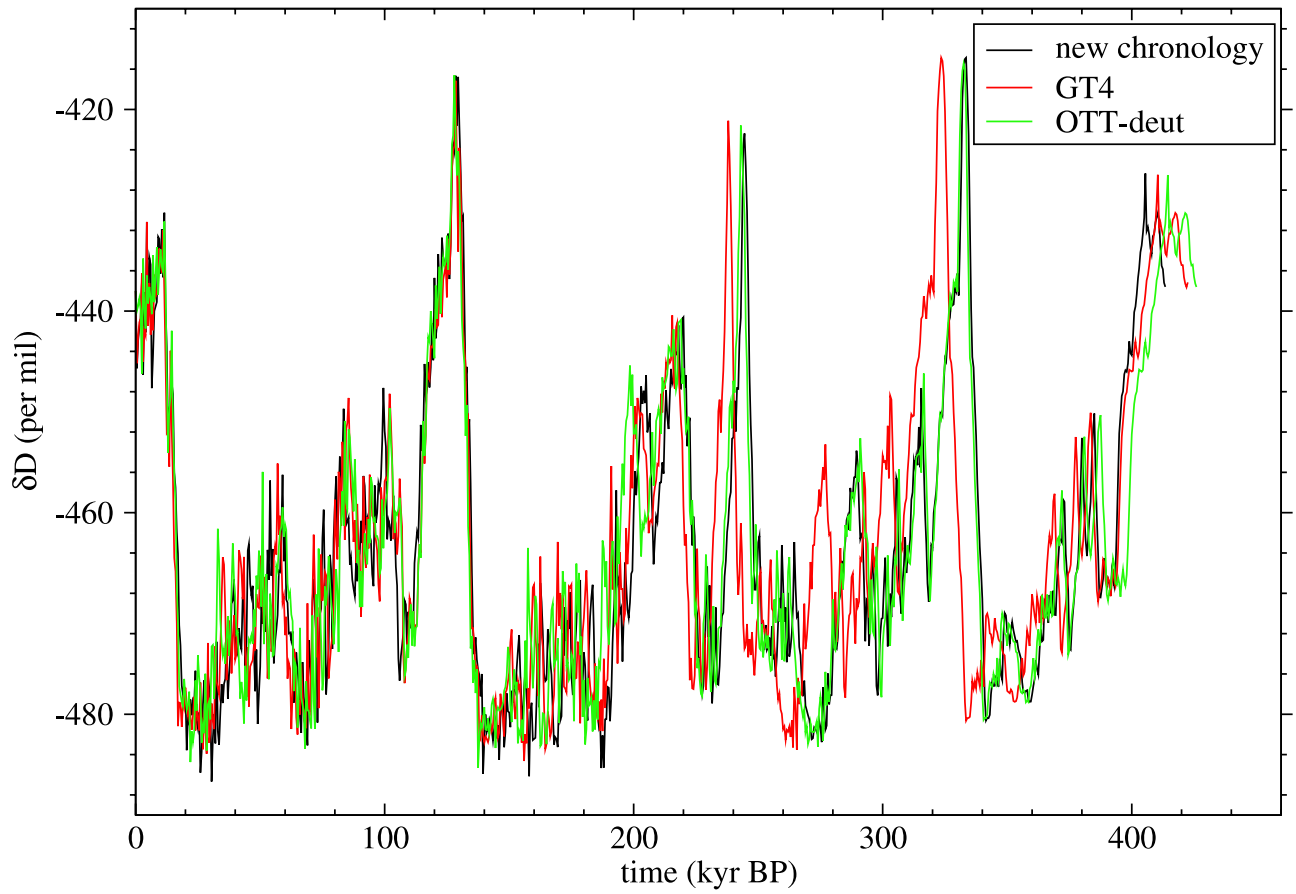

Figure 6. Optimal glaciological chronology obtained for the Vostok ice core compared with the previous glaciological chronology (GT4) and with the orbitally tuned chronology.

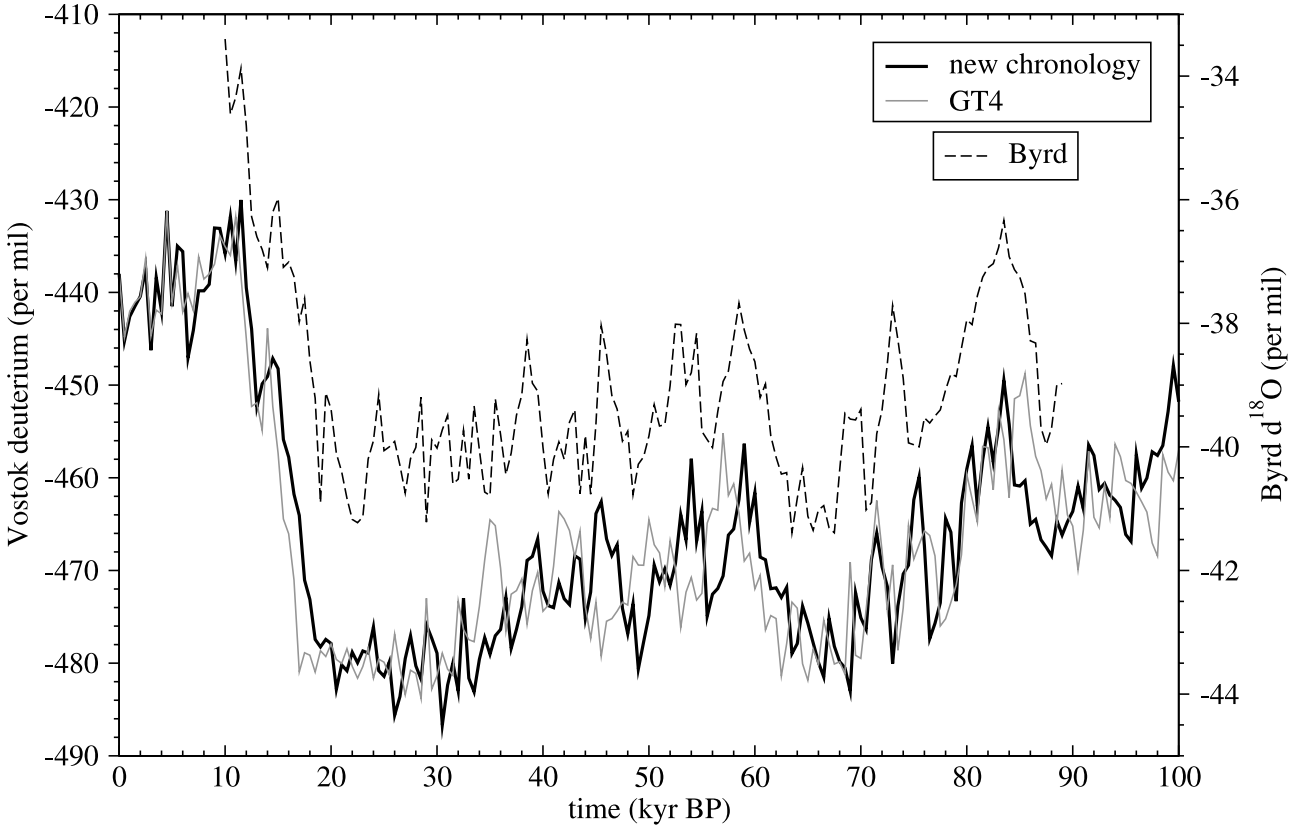

Figure 7. Comparison of Vostok isotopic record, dated either with the GT4 chronology or with the new chronology, and Byrd isotopic record dated by comparison to GISP2 via methane [*Blunier and Brook*, 2001].

ice core is strongly nonlinear: the influence of one parameter is not independent of the value of the other parameters.

4. New Parameterization of the Flow Line Upstream of Vostok

[22] An accurate topography of the Antarctic surface has been obtained by the ERS-1 satellite, with a spatial resolution of several kilometers and with an accuracy within a meter. With this topography, we derived the position of the flow line upstream of Vostok by following the greatest slope direction. Starting from Vostok, we computed iteratively the flow line position to Ridge B divide (see Figure 1). In fact, the correspondence between the ice flow line and the greatest slope direction is only valid at a large spatial scale because of shear stress effects at the local scale. Thus, to compute the greatest slope direction, the altimetric data were preliminary smoothed at a 100 km scale, as obtained by *Testut et al.* [2003] by comparison to GPS data. The greatest slope for a given position was then estimated with 4 neighboring points on a 20 km perpendicular grid. Two adjacent flow lines were also computed to evaluate divergence (or convergence) of ice flow.

[23] To evaluate the ice sheet thickness, we used an airborne radio echo sounding profile (see Figure 2) measured close to the Ridge B – Vostok ice flow line [*Siegert and Kwok*, 2000]. We have to note here that the position of this profile is not exactly the same as the position of our computed ice flow line (see Figure 1). The separation of these two lines is negligible around the Vostok lake area, but increases to 10–20 km for the majority of the flow line, and reaches 30 km at the ice divide, a distance sufficient to introduce an important error in our evaluation of ice thickness.

[24] We can distinguish several areas along the ice flow line (see Figures 2 and 3): (1) The dome area, with a length of ~70 km, is characterized by a roughly constant bedrock elevation of 800–1000 m above sea level and an ice thickness of ~2800–3000 m. There is a small divergence of ice flow in this area. (2) A first valley, extending from ~70 km to 100 km from the dome, where ice thickness reaches 3700 m. The divergence of ice flow is significant in this area. (3) A large mountain, from ~100 to ~140 km from Ridge B, where bedrock elevation reaches 1500 m. The small ice thickness leads to an important surface slope in this area. The divergence of ice flow is negligible. (4) A plateau, extending from ~140 to 240 km from Ridge B, where ice thickness and divergence of ice flow are intermediate. (5) The lake Vostok area, with a large ice thickness (~3800–3900 m). There is a convergent area at the western side of the lake, and a divergent area for the rest of the lake.

5. Using Chronological Control Points to Constrain the Dating

[25] The values of other previously poorly known parameters are derived from calibrating the model with age of

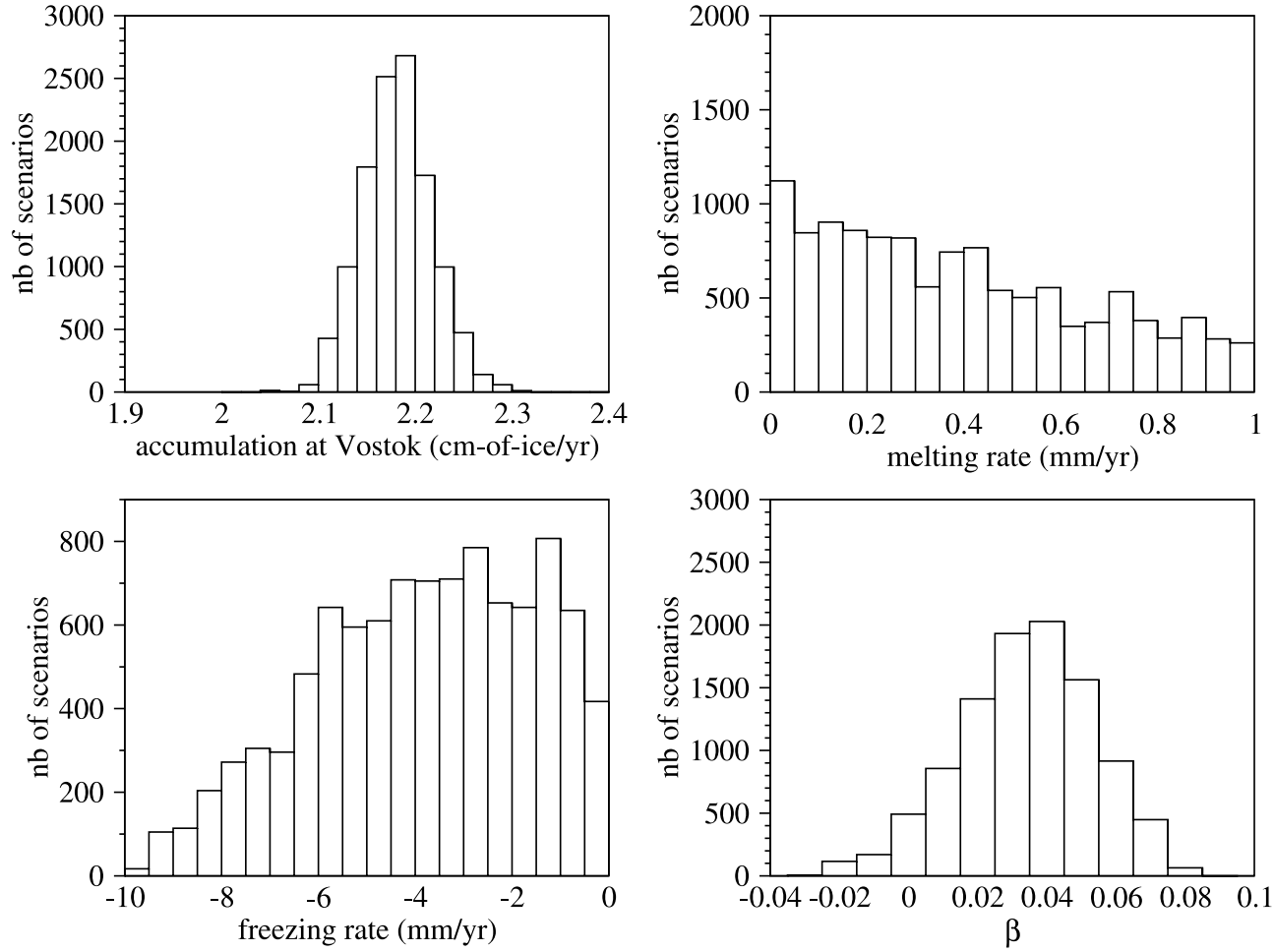

Figure 8. Bad known parameters reconstructed by the inverse method: present-day accumulation rate at Vostok site, melting rate upstream of Vostok lake, freezing rate above the Vostok lake, and β coefficient.

chronological tie points. We detail in this section all the tie points that can be used in the Vostok ice core.

5.1. Chronology of the Holocene by $^{14}C/^{10}Be$ Comparison

[26] Because the sources of productions are similar, carbon 14 and beryllium 10 exhibit similar variations of atmospheric fluxes during the past. Carbon 14 fluxes are well known for the last ~11,500 years thanks to the dendrochronology, which allows a very accurate dating. Beryllium 10 fluxes can be reconstructed with their concentration measured in the Vostok ice core, and these can be compared with the carbon 14 fluxes, allowing the dendrochronology age scale to be applied to the Vostok ice core [*Bard et al.*, 1997]. The $^{10}Be/^{14}C$ method is in fact only accurate for the Holocene period, where accumulation rates variations are low. Consequently, the Be10/C14 dating was performed for the last ~7,000 years [*Raisbeck et al.*, 1998]. From this analysis, we infer an age of 7180 yr at 178 m depth within the core.

5.2. Age of the ACR-Holocene Transition

[27] The depth of the Antarctic Cold Reversal (ACR) to Holocene transition at Vostok (275 m at mid transition) has been dated by isotopic matching (between Vostok and Byrd ice cores) and CH4 matching (between Byrd and GRIP ice cores) [*Blunier et al.*, 1998]. We deduce an age of 12.4 ± 0.4 kyr at the depth of 275 m at Vostok. The 0.4 kyr uncertainty is due to the uncertainty of the GRIP timescale, the inaccuracy of the Byrd/GRIP correlation, the uncertainty of the Byrd Δage evaluation, and the inaccuracy of the Byrd/Vostok isotopic correlation.

5.3. Age of the Beryllium 10 Peak

[28] A clear double peak in the beryllium 10 record at ~40,000 years is visible in all ice cores from Greenland and Antarctica covering this time period [*Raisbeck et al.*, 1987, 1992]. At Vostok, this event is centered at 601 m depth [*Raisbeck et al.*, 1987; *Yiou et al.*, 1997]. Moreover this event is synchronous with Dansgaard-Oeschger event number 10 [*Yiou et al.*, 1997], an event that has been identified in records from speleothems [*Wang et al.*, 2001; *Genty et al.*, 2003] and accurately dated by the uranium-thorium method. We thus use an control age of 41 ± 2 kyr at a depth of 601 m at Vostok.

5.4. Comparison With Orbital Variations

[29] A comparison of Vostok deuterium (δD) with insolation variations allows an orbitally tuned timescale to be constructed [*Parrenin et al.*, 2001], assuming a 3 kyr phase

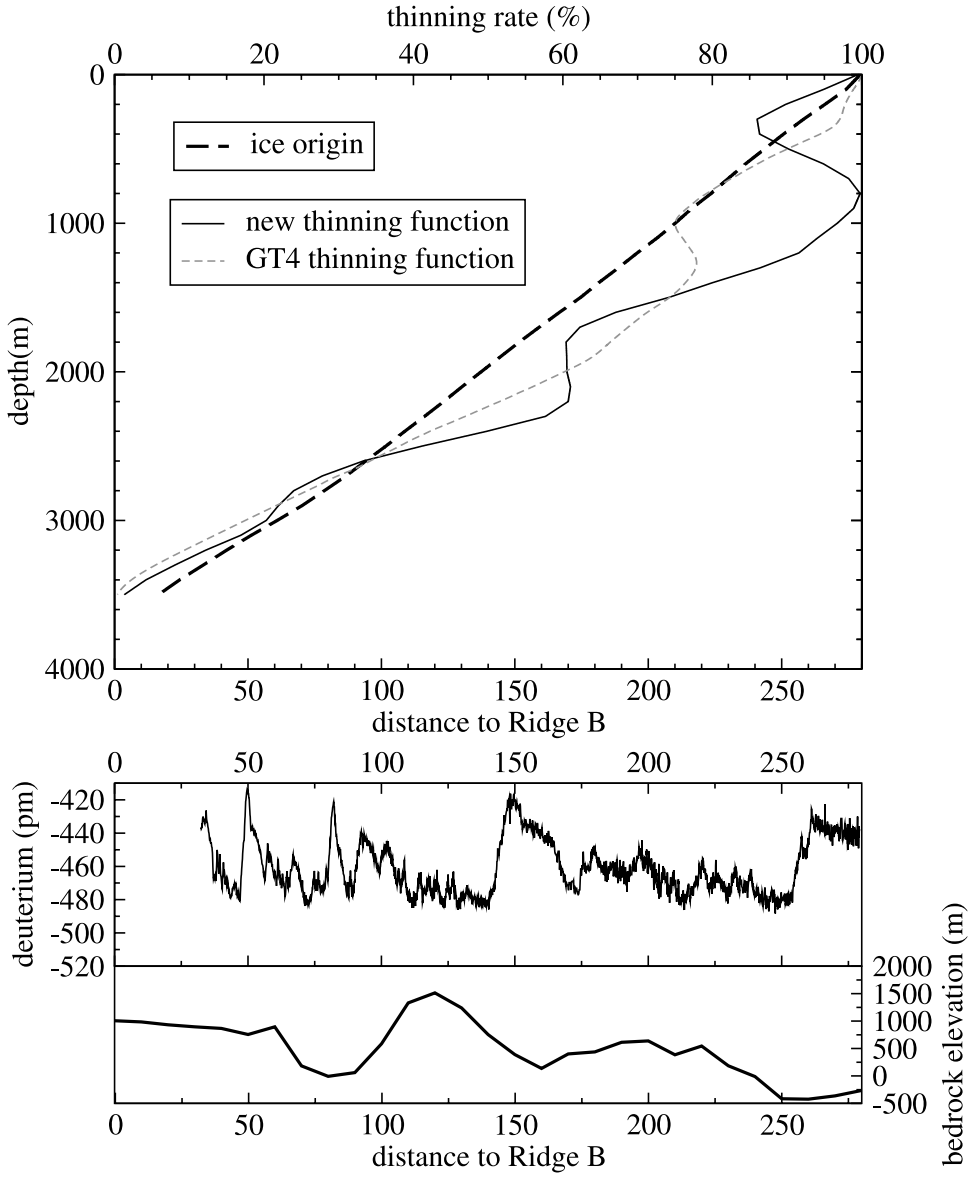

Figure 9. (top) Thinning function and ice origin (right) of the ice against depth in the Vostok deep drilling. (bottom) Bedrock elevation and ice deuterium against ice origin shown for comparison.

lag of deuterium with respect to June solstice insolation at 65°N. Of course, an important uncertainty is attached to such a chronology, resulting from (1) the inaccuracy of phase lag evaluation and (2) the assumption of a constant phase lag. However, if we suppose that we did not miss a precessional cycle in the δD record, this uncertainty does not exceed 6 kyr. It is thus the best way of obtaining a chronological constraint for the bottom part of the core. From this orbital timescale, we extracted 6 age control points where the deuterium record contains a clear precessional cycle (see Table 1).

6. Optimizing the Vostok Chronology

6.1. Hypotheses and Method

[30] The model used is described section 2. Spatial variations of accumulation upstream of Vostok are poorly known. The only information has been obtained by comparing the Dome B and Vostok ice cores isotopic data: *Ritz* [1992] deduced that accumulation rate at Dome B is 1.5 higher than at Vostok. However, our constraints on the Vostok chronology are not sufficiently accurate to reconstruct through the inverse method these variations of accumulation at a small spatial scale, but only at a regional scale. It is why we suppose that the $A^0(x)$ function is a second-order polynomial. Hence we have three free parameters in the horizontal accumulation profile. Concerning the sliding rate, we suppose that it is equal to 100% of total velocity inside the Vostok lake area (extending 40 km upstream of Vostok) and negligible elsewhere. We suppose that there is a freezing rate above lake Vostok (noted $-\dot{f}_1$), and a constant melting rate elsewhere (noted $\dot{f}_2$). Again, this is probably not the case but our accumulation-flow model is not sufficiently well constraint to resolve in details the melting rates upstream of the Vostok lake. Note that $-\dot{f}_1$ and $-\dot{f}_2$ are two free parameters of the model, the

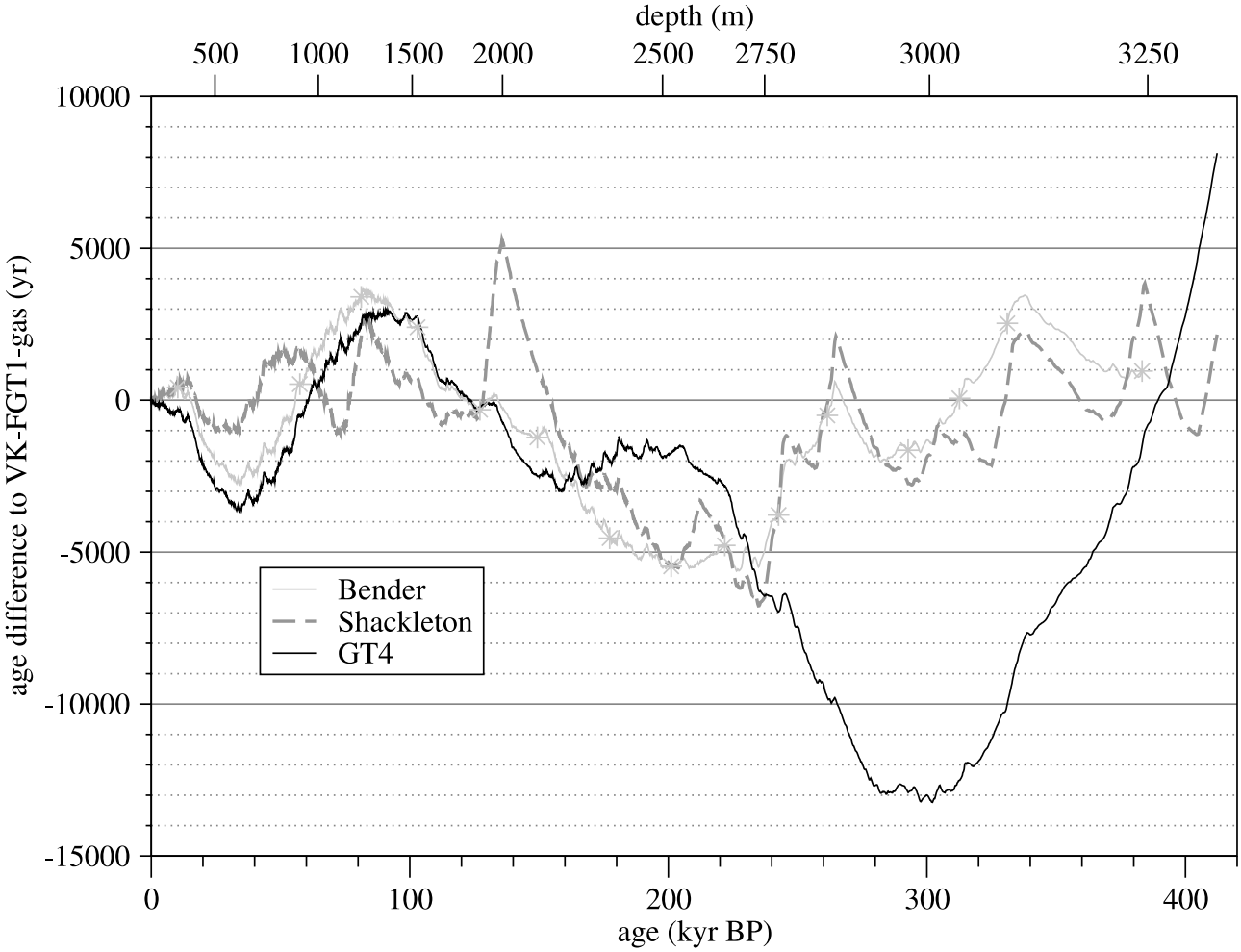

Figure 10. Comparisons of different Vostok timescales along four climatic cycles. GT4 is used as the reference timescale.

value of which will be determined by the inverse method. The *Sh* parameter (accounting for the ice flow divergence or convergence), and the bedrock and surface elevation have been obtained from satellite and airborne data (section 3). The *m* parameter of the velocity profile (see equation (6)) is fixed to 5 for the Ridge area (from 0 to 40 km far from Ridge B) and 10 for the rest of the ice flow line.

[31] Concerning the accumulation model, there are uncertainties in several relationships: the deuterium–surface temperature relationship, the surface temperature–inversion temperature relationship, and the inversion temperature–accumulation relationship. However, we are only able to constrain the accumulation rates through the chronological constraints, but not the temperature variations: letting all these relationships open (i.e., with free parameters), our inverse problem would be indeterminate. Consequently, we chose to fix the deuterium–surface temperature and surface temperature–inversion temperature relationships at their present day values, and to only let open the inversion temperature–accumulation relationship, through the β coefficient (see equation (7)). Moreover, this choice is validated by the independent confirmation of the deuterium–surface temperature relationship through various methods [*Jouzel et al.*, 2003]. Finally, we have six free parameters in our inverse experiment: four for the accumulation model and two for the thinning model.

[32] Our first inverse experiment uses the chronological information described in section 4 and summarized in Table 1. The chronological constraints are defined with Gaussian doors with a width equal to the uncertainty of the related control point. We have considered that the uncertainties of these control points are independent in terms of probability.

[33] The inverse method is described in detail by *Parrenin et al.* [2001] and *Parrenin* [2002]. Each inverse experiment is made of 10,000 tested scenarios. To initialize the forced walk (FW) algorithm, a first set of 1000 scenario is made in mode random walk and the matrix of covariance of the FW algorithm is initialized with the covariance obtained from this set of scenarios. Of these 10,000 scenarios, approximately 25% are accepted. To assess that we have tested a sufficient number of scenarios to obtain reliable statistics, we launch simultaneously three inverse experiments and verify if the obtained probabilistic reconstructions are close to each other.

6.2. Optimized Vostok Chronology

[34] The resulting optimized chronology is shown in Figures 6 and 7. On the four glacial cycles, the new chronol-

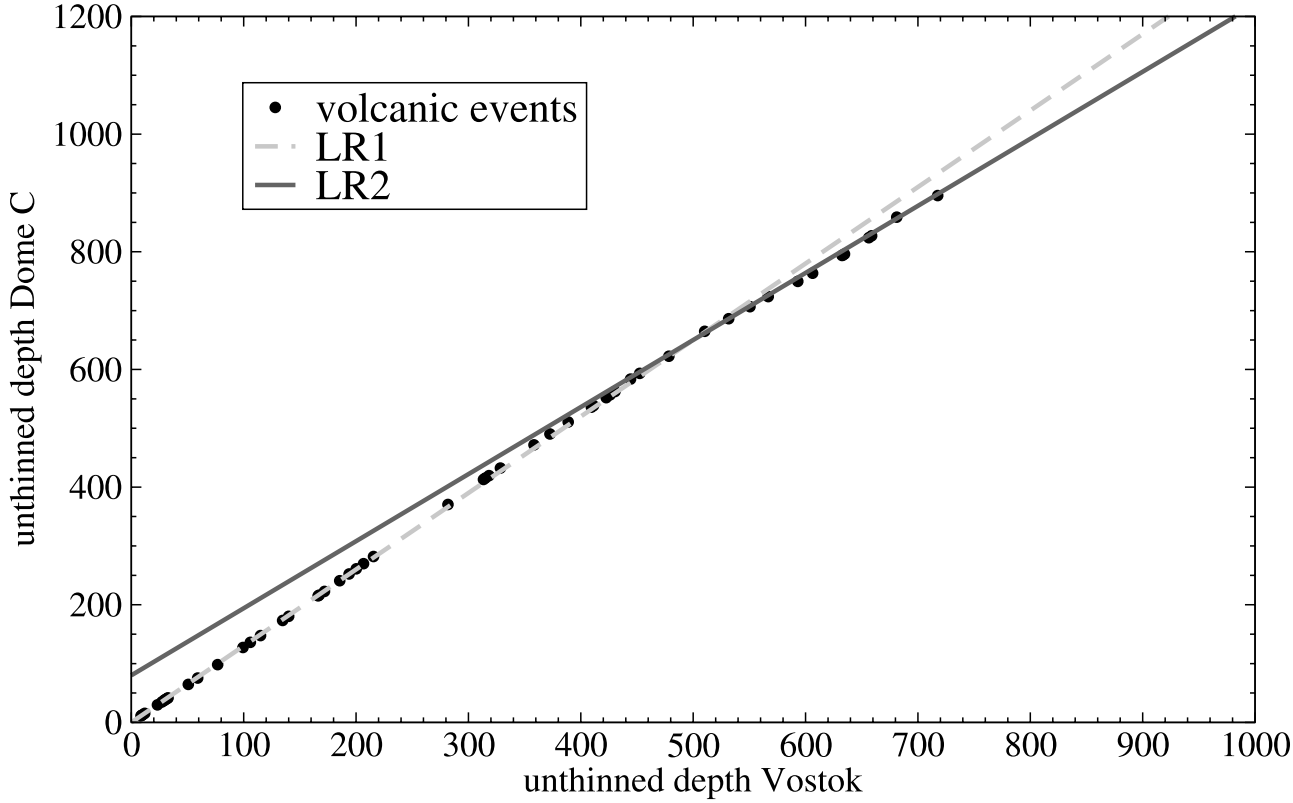

Figure 11. Depth to depth correlation between common volcanic signatures (145 events) recorded in EDC96 and Vostok ice cores. LR1 is linear regression for the first ~500 m (~20 kyr); LR2 is linear regression for the deeper core (20–45 kyr).

ogy is in good agreement with the orbital tuning chronology, contrary to the inverse chronology obtained with the old parameterization of the ice flow line [*Parrenin et al.*, 2001].

[35] This new chronology is also consistent with the beryllium 10 peak age (41 kyr). As a consequence, this chronology is in good agreement (within 2 kyr) with chronologies from Greenland ice cores. We thus believe that the confidence interval of our new chronology does not exceed 5% for the last glacial period.

[36] Concerning accumulation rates (see Figure 8), we found the β coefficient (see equation (7)) to be significantly positive, that is to say that glacial accumulation rates are significantly smaller than those expected from the present-day spatial relationship. These small glacial accumulation rates were also necessary to obtain consistent chronologies for Dome C and Dome Fuji [*Parrenin*, 2002].

[37] Ice origin and thinning from the best guessed experiment are shown on Figure 9. We see clearly that bedrock elevation has a major influence on the final thinning function, as expected. Concerning ice origin, (1) the Vostok lake corresponds mainly to ice from the Holocene and from the last deglaciation. (2) Ice from stage 5.5 roughly originates from a valley 140 to 170 km far from Ridge B. (3) The largest mountain in the bedrock profile mainly corresponds to ice from stages 6 and 7.1. (4) The largest depression in the bedrock profile corresponds to ice from stages 7.3, 7.5 and 8, which is why this time period is significantly expanded in this new chronology with respect to GT4.

[38] The reconstructed accumulation rate (see Figure 8) is 2.14 ± 0.04 cm of ice/yr for the Vostok site, 2.72 ± 0.29 cm of ice/yr at the middle between Ridge B and Vostok, and 3.01 ± 0.35 cm of ice/yr at Ridge B. This last value is consistent with the value obtained for the Dome B drilling site [*Ritz*, 1992]. Note also that the inverse procedure does not reconstruct accurately melting above the Vostok lake and freezing upstream (see Figure 8).

6.3. Comparison With Other Vostok Chronologies

[39] *Shackleton* [2000] and *Bender* [2002] [see also *Petit et al.*, 1999] produced two timescales for Vostok, both based on a orbital tuning of the oxygen 18 from air bubbles ($^{18}O_{atm}$) record. The Bender timescale was also checked independently with the O_2/N_2 ratio, a record very well correlated with local summer insolation [*Bender*, 2002]. The author estimates the uncertainty of his chronology at about 3 kyr.

[40] On Figure 10, we compared our new chronology with GT4, the Bender chronology and the Shackleton chronology. Concerning GT4, as said above, the two main features are that the new chronology is ~3 kyr older for the last glacial part between 30 and 60 kyr BP, and ~12 kyr older at ~300 kyr.

[41] The more important feature is the very good agreement between our new glaciological chronology and Shackleton and Bender timescales. The difference generally does not exceed 3.5 kyr, except for two intervals.

[42] The first one is at ~2000 m (~143 kyr), where the Shackleton timescale is older than VK-FGT1 by more than 7 kyr. However, the difference with Bender timescale does not exceed 2 kyr in this time interval. This feature is thus not robust.

[43] The second one is at ~2500 m (180–200 kyr) where the difference with both orbitally tuned chronologies reaches 5 kyr. However, the glaciological chronology is in very good agreement with the deuterium-based orbital tuning chronology (see Figure 6) in this time period. In conclusion, the new glaciological timescale is in agreement with the orbitally tuned chronologies within the limit of their confidence intervals. Therefore the confidence interval of our glaciological chronology does not exceed ~5 kyr for the whole record.

6.4. Dome C–Vostok Depth Comparison

[44] *Udisti et al.* [2004] derived 145 depth to depth correlations between Vostok and Dome C ice cores, based on common volcanic events. Using thinning functions from GT4 for Vostok and EDC1 for Dome C, they concluded that the ratio between Vostok and DC accumulation rates changed ~20 kyr ago.

[45] Because our new thinning profile for the Vostok ice core is significantly different from the one of GT4, we determine here if their conclusions are still valid with our new results. To this aim, we corrected Vostok and Dome C [*EPICA Community Members*, 2004] for the thinning factor, to obtain an unthinned depth in ice equivalent. Figure 11 shows the position of these volcanic events on a unthinned depth scale for Vostok and Dome C. If the ratio between Vostok and Dome C accumulation is constant through time, the relationship between unthinned depths is linear. On the contrary, if this relationship is not linear, thus the accumulation ration is not constant.

[46] As in the work by *Udisti et al.* [2004], we found a change in the slope at around 500 m. We calculated two linear regressions (LR1′ and LR2′) for the first ~500 m (corresponding to ~20 kyr) and from 500 m to bottom (from ~20 to ~45 kyr) encompassing the glacial period:

$$\mathrm{LR1'}:\ \mathrm{DC} = 1.30\ \mathrm{VK}$$

$$\mathrm{LR2'}:\ \mathrm{DC} = 80 + 1.14\ \mathrm{VK}$$

Compared to the two linear relationships LR1 and LR2 derived by Udisti et al., these two relationships are closer to each other. We still infer a change of 12% of the accumulation ratio, but less important than the value of 22% predicted by *Udisti et al.* [2004].

[47] However, we have to keep in mind that 500 m depth corresponds exactly to the lake Vostok boundary: ice above 500 m depth in the ice core originates from the lake Vostok area, whereas ice deeper originates upstream of it. What we interpret here as a change of accumulation ratio could thus comes from a poor estimation of the thinning in this part due to the mechanical effects of the lake boundary. Indeed, our simple model based on the simple shear layer approximation cannot represent with accuracy the mechanical history of the ice in this region. Thus this remaining change of accumulation ratio is still subject to uncertainties.

7. Conclusions

[48] In this article, we describe an accumulation-flow model that allows the determination of an ice core chronology, not necessarily at an ice dome. We show the strong influence of bedrock elevation and basal conditions upstream of the drilling site, in the thinning function, and the strong influence of ice flow divergence on the ice origin. We also show the strong nonlinear behavior of this model, and thus the necessity to use a Monte Carlo method to optimize this model.

[49] We derive a new parameterization of the Vostok ice flow line, using direct measurements of bedrock and surface elevation and a new depiction of ice flow divergence. With this new parameterization, and based on a Monte Carlo inverse method, we obtain a new Vostok ice core chronology that is more consistent with Greenland ice core chronologies for the last glacial part and more consistent with orbital tuning chronologies on the four glacial cycle of the deep ice core than previous chronologies.

[50] Further improvements could be made on the Vostok chronology. First, taking into account information from isochronous levels measured from radio echo sounding may allow us to better constrain the spatial variation of accumulation upstream of Vostok, influenced in particular by the redistribution of snow by wind at the surface. Second, our evaluation of ice thickness upstream of Vostok is only based on one radio echo sounding profile and the location of this profile does not fully coincide with the Vostok flow line. We need a more complete map of the bedrock topography in this area. Finally, information on the gas age – ice age difference could also help constraining accumulation rate, temperature, and the thinning factor.

Appendix A

[51]

$$\int_0^\zeta \Psi(\zeta')d\zeta' = \zeta\left(s + (1-s)\frac{m+2}{m+1}\left(1 - \frac{\zeta^{m+2}}{m+2}\right)\right)$$

$$\int_0^\zeta \frac{\partial\Psi}{\partial s}(\zeta')d\zeta' = \frac{\zeta}{m+1}\left(\zeta^{m+1} - 1\right)$$

$$\int_0^\zeta \frac{\partial\Psi}{\partial m}(\zeta')d\zeta' = \frac{(1-s)\zeta}{(m+1)^2}\left(-1 + \zeta^{m+1}(1 + (m+1)\ln(\zeta))\right)$$

$$\frac{\partial\Psi}{\partial x} = \frac{\partial\Psi}{\partial s}(\zeta)\frac{\partial s}{\partial x} + \frac{\partial\Psi}{\partial m}(\zeta)\frac{\partial m}{\partial x} + \frac{\partial\Psi}{\partial\zeta}(\zeta)\frac{\partial\zeta}{\partial x}$$

$$\frac{\partial\Psi}{\partial s}(\zeta) = \frac{1}{m+1}\left((m+2)\zeta^{m+1} - 1\right)$$

$$\frac{\partial\Psi}{\partial m}(\zeta) = \frac{1-s}{(m+1)^2}\left(-1 + \zeta^{m+1}(1 - (m+1)(m+2)\ln(\zeta))\right)$$

$$\left(\frac{\partial\Psi}{\partial\zeta}\frac{\partial\zeta}{\partial x}\right)(\zeta) = (1-s)(m+2)\zeta^m\frac{\zeta\dfrac{\partial H}{\partial x} - \dfrac{\partial E}{\partial x}}{H}$$

[52] **Acknowledgments.** We thank Nicolas Lhomme and Nick Shackleton for helpful discussions. This work is part of the POP (Pole-Ocean-Pole) and PNEDC (Projet National pour l'Étude de la Dynamique du Climat) projects. UK-NERC grant NER/A/S/2001/01011.

References

Arnaud, L., J.-M. Barnola, and P. Duval (2000), Physical modeling of the densification of snow/firn and ice in the upper part of polar ice sheets, in *Physics of Ice Core Records*, edited by T. Hondoh, pp. 285–305, Hokkaido Univ. Press, Sapporo, Japan.

Bard, E., G. M. Raisbeck, F. Yiou, and J. Jouzel (1997), Solar modulation of cosmogenic nuclide production over the last millennium: Comparison between ^{14}C and ^{10}Be records, *Earth Planet. Sci. Lett.*, *150*, 453–462.

Bender, M. L. (2002), Orbital tuning chronology for the Vostok climate record supported by trapped gas composition, *Earth Planet. Sci. Lett.*, *204*, 275–289.

Blunier, T., and E. J. Brook (2001), Timing of millennial-scale climate change in Antarctica and Greenland during the last glacial period, *Science*, *291*, 109–112.

Blunier, T., et al. (1998), Asynchrony of Antarctic and Greenland climate change during the last glacial period, *Nature*, *394*, 739–743.

Connolley, W. M. (1996), The Antarctic temperature inversion, *Int. J. Climatol.*, *16*, 1333–1342.

Drewry, D. J. (Ed.) (1983a), The surface of the Antarctic Ice Sheet, in *Antarctica*: *Glaciological and Geophysical Folio*, sheet 2, Scott Polar Res. Inst., Cambridge, U. K.

Drewry, D. J., (Ed.) (1983b), The bedrock surface of Antarctica, in *Antarctica*: *Glaciological and Geophysical Folio*, sheet 3, Scott Polar Res. Inst., Cambridge, U. K.

EPICA Community Members (2004), 8 glacial cycles from an Antarctic ice core, *Nature*, *429*, 623–628.

Genty, D., D. Blamart, R. Ouhadi, M. Gilmour, A. Baker, J. Jouzel, and S. Van-Exter (2003), Precise dating of Dansgaard-Oeschger climate oscillations in western Europe from stalagmite data, *Nature*, *421*, 833–837.

Hutter, K. (1983), *Theoretical Glaciology*, D. Reidel, Norwell, Mass.

Imbrie, J., et al. (1992), On the structure and origin of major glaciation cycles: 1. Linear responses to Milankovitch forcing, *Paleoceanography*, *7*(6), 701–738.

Jouzel, J., F. Vimeux, N. Caillon, G. Delaygue, G. Hoffmann, V. Masson, and F. Parrenin (2003), Magnitude of isotope/temperature scaling for interpretation of central Antarctic ice cores, *J. Geophys. Res.*, *108*(D12), 4361, doi:10.1029/2002JD002677.

Lorius, C., and L. Merlivat (1977), Distribution of mean surface stable isotope values in East Antarctica. Observed changes with depth in a coastal area, in *Isotopes and Impurities in Snow and Ice: Proceedings of the Grenoble Symposium*, *IAHS Publ.*, *118*, 125–137.

Parrenin, F. (2002), Datation glaciologique des forages profonds en Antarctique et modélisation conceptuelle des paléoclimats: Implications pour la théorie astronomique des paléoclimats, Ph.D. thesis, Univ. J. Fourier, Grenoble, France.

Parrenin, F., J. Jouzel, C. Waelbroeck, C. Ritz, and J.-M. Barnola (2001), Dating the Vostok ice core by an inverse method, *J. Geophys. Res.*, *106*(D23), 31,837–31,851.

Petit, J. R., et al. (1999), Climate and atmospheric history of the past 42,000 years from the Vostok ice core, Antarctica, *Nature*, *399*, 429–436.

Raisbeck, G. M., F. Yiou, D. Bourles, C. Lorius, J. Jouzel, and N. I. Barkov (1987), Evidence for two intervals of enhanced ^{10}Be deposition in Antarctic ice during the last glacial period, *Nature*, *326*, 273–277.

Raisbeck, G. M., F. Yiou, J. Jouzel, J. R. Petit, E. Bard, and N. I. Barkov (1992), ^{10}Be deposition at Vostok, Antarctica, during the last 50,000 years and its relationship to possible cosmogenic production variations during this period, in *The Last Deglaciation: Absolute and Radiocarbon Chronologies*, edited by E. Bard and W. S. Broecker, pp. 127–139, Springer-Verlag, New York.

Raisbeck, G. M., F. Yiou, E. Bard, D. Dollfus, J. Jouzel, and J. R. Petit (1998), Absolute dating of the last 7000 years of the Vostok ice core using ^{10}Be, *Mineral. Mag.*, *62A*, 1228.

Rémy, F., P. Shaeffer, and B. Legrésy (1999), Ice flow physical processes derived from the ERS-1 high-resolution map of the Antarctica and Greenland ice sheets, *Geophys. J. Int.*, *139*, 645–656.

Richardson, C., E. Aarholt, S.-E. Hamran, P. Holmlund, and E. Isaksson (1997), Spatial distribution of snow in western Dronning Maud Land, East Antarctica, mapped by ground-based snow radar, *J. Geophys. Res.*, *102*(B9), 20,343–20,353.

Ritz, C. (1992), Un modèle thermo-mécanique d'évolution pour le bassin glaciaire antarctique Vostok-glacier Byrd: Sensibilité aux valeurs des paramètres mal connus, thèse d'état, Univ. J. Fourier, Grenoble, France.

Ritz, C., V. Rommelaere, and C. Dumas (2001), Modeling the Antarctic ice sheet evolution of the last 42,0000 years: Implication for altitude changes in the Vostok region, *J. Geophys. Res.*, *106*(D23), 31,943–31,964.

Shackleton, N. J. (2000), The 10,0000-year ice-age cycle identified and found to lag temperature, carbon dioxide, and orbital eccentricity, *Science*, *289*, 1897–1902.

Siegert, M. J., and R. Kwok (2000), Ice-sheet radar layering and the development of preferred crystal orientation fabrics between Lake Vostok and Ridge B, central East Antarctica, *Earth Planet. Sci. Lett.*, *179*(2), 227–235.

Testut, T., R. Hurd, R. Coleman, F. Rémy, and B. Legrésy (2003), Comparison between computed balance velocities and GPS measurements in the Lambert Glacier basin, East Antarctica, *Ann. Glaciol.*, *37*, 337–343.

Udisti, R., S. Becagli, E. Castellano, B. Delmonte, J. Jouzel, J.-R. Petit, J. Schwander, B. Stenni, and E. W. Wolff (2004), Stratigraphic correlations between the European Project for Ice Coring in Antarctica (EPICA) Dome C and Vostok ice cores showing the relative variations of snow accumulation over the past 45 kyr, *J. Geophys. Res.*, *109*, D08101, doi:10.1029/2003JD004180.

Wang, Y. J., H. Cheng, R. L. Edwards, Z. S. An, J. Y. Wu, C. C. Shen, and J. A. Dorale (2001), A high-resolution absolute-dated late Pleistocene Monsoon record from Hulu Cave, China, *Science*, *294*, 2345–2348.

Yiou, F., et al. (1997), Beryllium 10 in the Greenland Ice Core Project ice core at Summit, Greenland, *J. Geophys. Res.*, *102*, 26,783–26,794.

F. Parrenin and F. Rémy, Laboratoire d'Etudes en Geophysique et Océanographie Spatiales, 31400 Toulouse, France. (parrenin@notos.cst.cnes.fr)

C. Ritz, Laboratoire de Glaciologie et Géophysique de l'Environnement, 54, rue Molière, 38400 Saint Martin d'Hères, France.

M. J. Siegert, Bristol Glaciology Centre, School of Geophysical Sciences, Bristol BS8 1SS, UK.

J. Jouzel, IPSL/Laboratoire des Sciences du Climat et de l'Environnement, 91191 Gif-sur-Yvette, France.